ChemPubSoc Europe

DOI: 10.1002/chem.201xxxxxx

CHEMISTRY
A European Journal
Full Paper

Luminescent $Pt^{IV}$ complexes

# Exploring Excited-State Tunability in Luminescent Tris-cyclometalated Platinum(IV) Complexes: Synthesis of Heteroleptic Derivatives and Computational Calculations

Fabio Juliá,[a] Gabriel Aullón[b], Delia Bautista[c] and Pablo González-Herrero*[a]

**Abstract:** The synthesis, structure, electrochemistry, and photophysical properties of a series of heteroleptic tris-cyclometalated $Pt^{IV}$ complexes are reported. The complexes *mer*-[Pt(C^N)$_2$(C'^N')]OTf, with C^N = *C*-deprotonated 2-(2,4-difluorophenyl)pyridine (dfppy) or 2-phenylpyridine (ppy), and C'^N' = *C*-deprotonated 2-(2-thienyl)pyridine (thpy) or 1-phenylisoquinoline (piq), were obtained by reacting bis-cyclometalated precursors [Pt(C^N)$_2$Cl$_2$] with 2 equiv of AgOTf and an excess of the N'^C'H pro-ligand. The complex *mer*-[Pt(dfppy)$_2$(ppy)]OTf was obtained analogously and photoisomerized to its *fac* counterpart. The new complexes display long-lived luminescence at room temperature in the blue to orange color range. The emitting states involve electronic transitions almost exclusively localized on the ligand with the lowest $\pi$-$\pi^*$ energy gap and have very little metal character. DFT and TD-DFT calculations on *mer*-[Pt(ppy)$_2$(C'^N')]$^+$ (C'^N' = thpy, piq) and *mer/fac*-[Pt(ppy)$_3$]$^+$ support this assignment and provide a basis for the understanding of the luminescence of tris-cyclometalated $Pt^{IV}$ complexes. Excited states of LMCT character may become thermally accessible from the emitting state in the *mer* isomers containing dfppy or ppy as chromophoric ligands, leading to strong nonradiative deactivation. This effect does not operate in the *fac* isomers or the *mer* complexes containing thpy or piq, for which nonradiative deactivation originates mainly from vibrational coupling to the ground state.

## Introduction

The development of transition-metal complexes that exhibit triplet excited states with very long lifetimes has been motivated by their potential applicability as photoredox catalysts in solar energy conversion processes[1] and organic synthesis,[2] lifetime-based chemosensors for bioimaging,[3] and photosensitizers for singlet-oxygen generation and photodynamic chemotherapy.[4] Luminescent complexes of second- and third-row late-transition metals with heteroaromatic ligands, *i.e.*, polypyridines, cyclometalating arylpyridines or related compounds, may exhibit triplet metal-to-ligand charge-transfer (MLCT), ligand-centered (LC or $\pi$-$\pi^*$), or mixed LC/MLCT emitting states.[5] The characteristics of these states greatly depend on the degree of metal orbital contribution to the involved frontier orbitals, mainly because the strong spin-orbit coupling (SOC) induced by heavy transition metals promotes intersystem-crossing (ISC) from the lowest singlet excited state ($S_1$) to the triplet state ($T_1$) and also accelerates the radiative transition from $T_1$ to the ground state ($S_0$).[6] Therefore, triplet excited states of mainly MLCT character usually exhibit higher radiative rate constants and shorter emission lifetimes than those of predominantly LC character. Accordingly, the excited-state lifetimes in $Ir^{III}$, $Pt^{II}$ or $Os^{II}$ complexes with heteroaromatic ligands increase as the influence of the metal is attenuated, either by lowering the energy of the occupied d orbitals through the use of $\pi$-accepting ancillary ligands,[6b, 7] or by introducing chromophoric ligands with more extended $\pi$-systems,[8] which make the emitting state behave more like an organic triplet, resulting in lower $T_1 \rightarrow S_0$ decay rates. Prolonging the lifetimes of $^3$MLCT states in $Ru^{II}$ polypyridine complexes has been a particularly active goal since the discovery that these states can participate in bimolecular electron-transfer reactions,[1] and lifetimes of the order of 100 $\mu$s have been attained by extending the $\pi$-delocalization on the heteroaromatic ligands[9] or through excited-state equilibration with $^3$LC states of pendant organic chromophores.[4a, 10]

In recent years, cyclometalated $Au^{III}$ [11] or $Pd^{II}$ [12] complexes are being increasingly investigated as triplet emitters with very long radiative lifetimes; the excited states in these complexes have very little metal character, because of the low energy of the occupied d

[a] *F. Juliá, Dr. P. González-Herrero*
*Departamento de Química Inorgánica, Facultad de Química*
*Universidad de Murcia, Apdo. 4021, 30071 Murcia (Spain)*
*Fax: (+) 34 868 884148*
*E-mail: pgh@um.es*

[b] *Dr. G. Aullón*
*Department de Química Inorgànica*
*Facultat de Química, Universitat de Barcelona*
*Martí Franquès, 1-11, 08028 Barcelona, Spain*

[c] *Dr. D. Bautista*
*SAI, Universidad de Murcia, Apdo. 4021, 30071 Murcia (Spain)*

*Supporting information for this article is available on the WWW under http://www.chemeurj.org/ or from the author.*

orbitals. Although cyclometalated $Pt^{IV}$ complexes fall in this category, studies on their excited-state properties are very limited.[13] Recently, we have reported the synthesis of a series of meridional and facial isomers of homoleptic tris-cyclometalated $Pt^{IV}$ complexes, *mer/fac*-$[Pt(C^N)_3]^+$, containing *C*-deprotonated 2-phenylpyridine (ppy), 2-(*p*-tolyl)pyridine (tpy), 2-(2,4-difluorophenyl)pyridine (dfppy), or 1-phenylpyrazole (ppz) as ligands.[14] The facial isomers exhibit high-energy (blue) emissions from $^3$LC states, characterized by lifetimes in the hundreds of microseconds range and quantum yields up to 0.49 in fluid solution at room temperature. In addition, they exhibit a highly oxidizing character in the excited state. This combination of photophysical and redox properties is unique among complexes of $d^6$ ions with heteroaromatic ligands and might find application in photocatalysis and other areas. For this reason, we believe that further developments involving the derivatization of tris-cyclometalated $Pt^{IV}$ complexes and the study of their photophysical properties are promising.

An adequate assessment of the applicability of tris-cyclometalated $Pt^{IV}$ complexes in different areas requires an exploration of their color tunability. In particular, lower absorption energies are desirable for visible-light photocatalysis or bioimaging. With this in mind, we set out to synthesize tris-cyclometalated $Pt^{IV}$ complexes containing cyclometalating ligands with lower $\pi$-$\pi^*$ transition energies. Such low energies are often achieved through the incorporation of electron-donating sulfur-containing heterocycles and/or extended $\pi$-systems.[15] For the present study, we have chosen 2-(2-thienyl)pyridine (thpy) and 1-phenylisoquinoline (piq), which have been widely employed to achieve emissions in the green to red color range from cyclometalated $Ir^{III}$,[16] $Pt^{II}$ [17] or $Au^{III}$ [18] complexes. Our efforts have led to the synthesis of a family of heteroleptic tris-cyclometalated $Pt^{IV}$ complexes containing two dfppy or ppy ligands and one thpy or piq ligand, which absorb at relatively low energies and exhibit long-lived emissions in the yellow to orange range. In addition, an heteroleptic dfppy/ppy complex is reported, which adds to the existing family of blue-emitting $Pt^{IV}$ complexes. We also include their electrochemical characterization and DFT/TD-DFT calculations on two representative heteroleptic complexes as well as the previously reported homoleptic complexes *mer*/*fac*-$[Pt(ppy)_3]^+$, which provide a better understanding of the underlying factors that determine the photophysical properties of tris-cyclometalated $Pt^{IV}$ complexes.

## Results and Discussion

### Synthesis

We have previously shown that the reactions of bis-cyclometalated precursors of the type $[Pt(C^N)_2Cl_2]$ with 2 equiv of AgOTf and an excess of the N^CH ligand in non-coordinating solvents give *mer* isomers of homoleptic tris-cyclometalated $Pt^{IV}$ complexes *mer*-$[Pt(C^N)_3]$OTf (C^N = ppy, tpy, dfppy, ppz) (Scheme 1).[14] The corresponding strongly emissive *fac* isomers were obtained by photoisomerization. For the present study, we attempted to prepare homoleptic *mer* isomers containing thpy or piq as cyclometalating ligands by reacting $[Pt(thpy)_2Cl_2]$ (**2c**) or $[Pt(piq)_2Cl_2]$ (**2d**)] with 2 equiv of AgOTf and an excess of the corresponding N^CH pro-ligand. However, these reactions resulted in mixtures containing $Pt^{II}$ products. In the case of the piq ligand, the major product was $[Pt(piq)(piqH)_2]$OTf (**4d**), which could be isolated and characterized, while the thpy ligand led to a complex mixture in which the cations $[Pt(thpy)(thpyH)_2]^+$ and *mer*-$[Pt(thpy)_3]^+$ were detected by mass spectroscopy as minor products but could not be isolated.

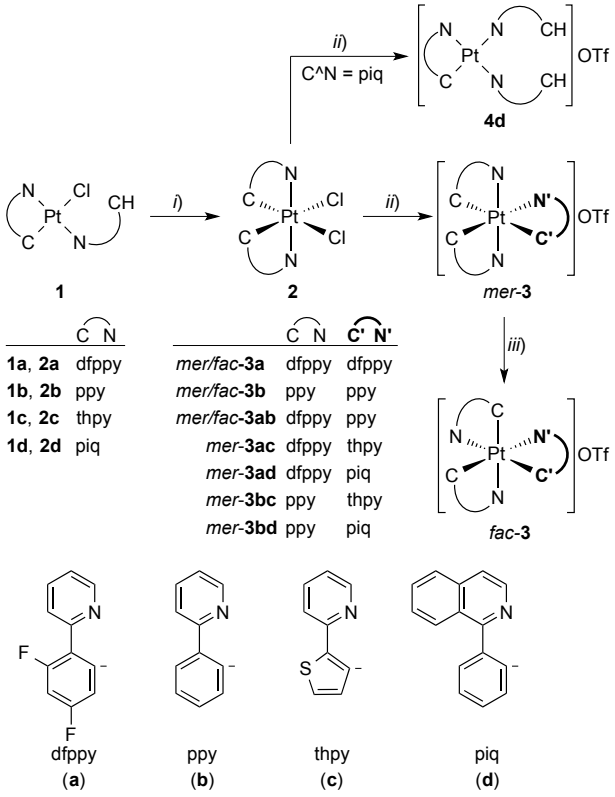


**Scheme 1.** Synthesis of tris-cyclometalated $Pt^{IV}$ complexes: i) $PhICl_2$, $CH_2Cl_2$; ii) 2 AgOTf, excess **N'^C'**H, $CH_2ClCH_2Cl$ (90 °C) or 1,2-$C_6H_4Cl_2$ (140 °C); c) h$\nu$, MeCN.

It thus became apparent that the synthesis of the homoleptic meridional isomers with thpy or piq ligands is not possible using this procedure because reduction to $Pt^{II}$ occurs at some stage. We then attempted the synthesis of heteroleptic tris-cyclometalated complexes by reacting complexes $[Pt(dfppy)_2Cl_2]$ (**2a**) or $[Pt(ppy)_2Cl_2]$ (**2b**)] with 2 equiv of AgOTf and a an excess of thpyH or piqH. These reactions led to *mer*-$[Pt(C^N)_2(C'^N')]$OTf, where C^N = dfppy and C'^N' = thpy (*mer*-**3ac**), piq (*mer*-**3ad**), or C^N = ppy and C'^N' = thpy (*mer*-**3bc**), piq (*mer*-**3bd**) (Scheme 1), which were isolated in moderate to good yields. In addition, the complex *mer*-$[Pt(dfppy)_2(ppy)]$OTf (*mer*-**3ab**) was synthesized following an analogous procedure in order to compare its properties with those of the heteroleptic complexes containing thpy or piq.

Following the synthetic route used for the homoleptic complexes,[14] we carried out irradiations of dilute acetonitrile solutions of the heteroleptic *mer* complexes with UV light in order to obtain the corresponding *fac* isomers through photoisomerization. Complex *mer*-**3ab** cleanly isomerized to *fac*-**3ab** in good yield (see Supporting Information for details). However,

irradiation of the thpy or piq derivatives led to mixtures of unidentified compounds.

## Crystal structures

The crystal structures of *mer*-**3ab**·2Et$_2$O and *mer*-**3ac**·Et$_2$O were solved by single crystal X-ray diffraction studies. The molecular structures of the cations are shown in Figures 1 and 2 and selected bond distances and angles are given in Table 1. In both cases the octahedral coordination around the Pt center is slightly distorted because of the narrow bite angle of the cyclometalating ligands [C–Pt–N angles in the range 79.14–81.49°]. The Pt–N bond in trans to a difluorophenyl group is *ca.* 0.10 Å longer than the mutually trans Pt–N bonds, because of the strong trans influence of the aryl group. For the same reason, the mutually trans Pt–C bonds are *ca.* 0.06–0.08 Å longer than the Pt–C bond in trans to a pyridyl. The cations of *mer*-**3ab** form inversion-related dimers through non-classical hydrogen bonds between the H4 atoms of the difluorophenyl groups and the Et$_2$O molecules (see the Supporting Information).

**Table 1.** Selected bond distances [Å] and angles [°] for *mer*-**3ab**·2Et$_2$O and *mer*-**3ac**·Et$_2$O.

| | *mer*-**3ab**·2Et$_2$O | *mer*-**3ac**·Et$_2$O |
|---|---|---|
| Pt1-C1 | 2.010(4) | 2.055(3) |
| Pt1-N1 | 2.026(3) | 2.034(2) |
| Pt1-N2 | 2.033(3) | 2.028(2) |
| Pt1-C21 | 2.063(4) | 2.003(3) |
| Pt1-C41 | 2.080(4) | 2.078(3) |
| Pt1-N3 | 2.122(3) | 2.142(2) |
| | | |
| C1-Pt-N1 | 81.40(15) | 81.08(11) |
| C21-Pt-N2 | 80.72(15) | 81.49(11) |
| C41-Pt-N3 | 79.60(15) | 79.14(11) |

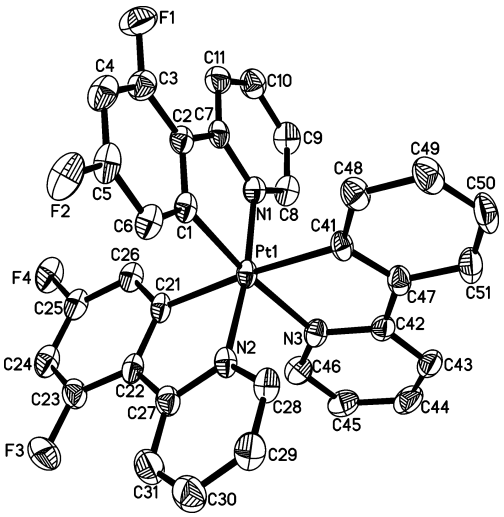


**Figure 1**. Thermal ellipsoid plot (50% probability) of the cation of *mer*-**3ab**. Hydrogen atoms are omitted for clarity.

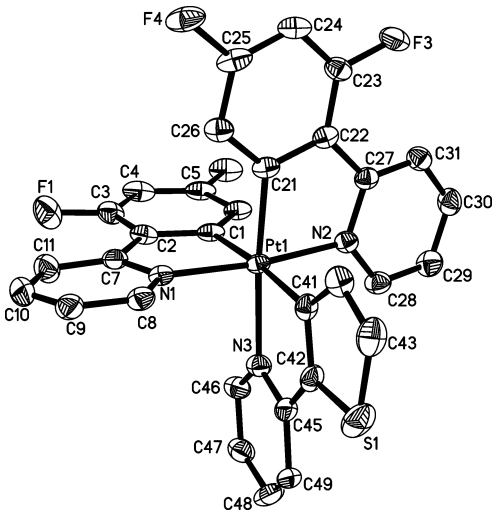


**Figure 2**. Thermal ellipsoid plot (50% probability) of the cation of *mer*-**3ac**. Hydrogen atoms are omitted for clarity.

## Electronic absorption spectra

The UV-visible absorption data of the series of complexes **2** and **3** in $CH_2Cl_2$ solution at 298 K are summarized in Table 2. Compounds **2** show several bands in the range 230–400 nm which can be ascribed to ligand-centered transitions ($^1$LC or $^1\pi$-$\pi^*$). As expected, the absorptions of **2c** and **2d** appear at significantly lower energies relative to **2a** and **2b**. The tris-cyclometalated compounds *mer*-**3** and *fac*-**3ab** show more complicated spectra, which appear to be approximately the superimposition of the absorptions arising from the different ligands. To illustrate this, the absorption spectra of *mer*-**3ac** and *mer*-**3ad** are compared in Figure 3 with those of **2a** and **2c**, or **2a** and **2d**, respectively, which can be taken as representative of the absorptions of each cyclometalating ligand. The absorption bands of *fac*-**3ab** are sharper and of slightly higher energies as compared to *mer*-**3ab**, just as observed for the homoleptic derivatives *mer*/*fac*-**3a** and **b**.[14] None of the complexes exhibits solvatochromic absorptions, which suggests that the involved electronic transitions have little or no charge-transfer character.

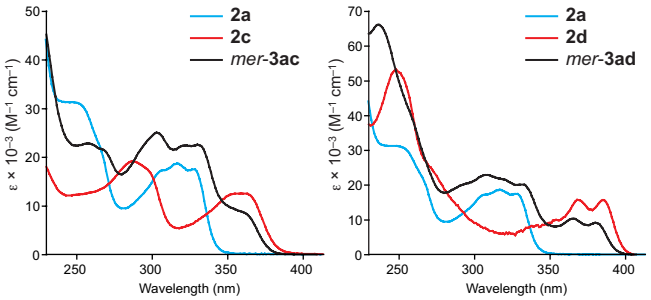


**Figure 3**. Absorption spectra of *mer*-**3ac** (left) and *mer*-**3ad** (right) compared with those of complexes **2a**, **2c** and **2d**.

**Table 2.** Electronic absorption data for the series of complexes **2** and **3** in $CH_2Cl_2$ solution (ca. $1 \times 10^{-5}$ M) at 298 K

| Complex | $\lambda_{max}$/nm ($\varepsilon \times 10^{-3}$/M$^{-1}$ cm$^{-1}$) |
|---|---|
| **2a** | 252 (31.1), 305 (17.2), 316 (18.9), 328 (17.7) |
| **2b** | 259 (20.9), 308 (12.1), 323 (10.7), 334 (10.6) |
| **2c** | 287 (19.3), 361 (12.7) |
| **2d** | 249 (52.8), 368 (15.6), 384 (15.8) |
| *mer*-**3a**[a] | 260 (25.4), 314 (24.7), 327 (22.0, sh) |
| *fac*-**3a**[a] | 260 (25.0), 312 (27.7), 323 (22.9, sh) |
| *mer*-**3b**[a] | 267 (29.7), 310 (25.6), 330 (18.6), 342 (13.2, sh) |
| *fac*-**3b**[a] | 270 (30.6), 309 (27.2), 320 (24.4), 330 (20.3, sh) |
| *mer*-**3ab** | 261 (28.3), 316 (26.8), 330 (22.2, sh) |
| *fac*-**3ab** | 263 (22.0), 311 (23.6), 323 (19.4, sh) |
| *mer*-**3ac** | 258 (22.8), 267 (21.4, sh), 302 (25.1), 321 (22.3), 330 (22.5), 361 (8.5, sh) |
| *mer*-**3ad** | 236 (66.3), 307 (23.0), 332 (20.1, sh), 364 (10.3), 380 (9.1) |
| *mer*-**3bc** | 271 (44.4), 298 (43.5), 306 (42.7), 341 (37.2), 360 (17.6, sh) |
| *mer*-**3bd** | 236 (29.0), 310 (9.6), 343 (7.7), 362 (4.9, sh), 380 (3.8) |

[a] Data from ref. [14].

## Luminescence

The emission data of the heteroleptic complexes **3** are summarized in Table 3. The data for the previously reported homoleptic dfppy and ppy *fac* isomers are also included for comparison. All of them exhibit structured emissions in deaerated $CH_2Cl_2$ solutions at 298 K, which become appreciably sharper and more intense in PrCN frozen glasses at 77 K. Emission lifetimes are in the order of tens or hundreds of microseconds at 298 K and hundreds of microseconds at 77 K. These characteristics, together with the observed large Stokes shifts (~8000 cm$^{-1}$), are indicative of phosphorescent emissions from excited states of essentially $^3$LC character. Fluorescence emissions are not observed, except for the piq derivatives *mer*-**3ad** and *mer*-**3bd** (see below), which indicates that intersystem crossing is very effective in most cases and suggests that metal orbital involvement in the excited state is at a critical level.

The heteroleptic facial isomer *fac*-**3ab** is a very efficient emitter in $CH_2Cl_2$ solution at 298 K ($\Phi$ = 0.43), in line with the homoleptic complexes *fac*-**3a** and *fac*-**3b** previously reported by us.[14] Its emission spectrum is very similar to that of the ppy complex *fac*-**3b**,[14] suggesting that the responsible electronic transition is confined within the ppy ligand, which has a lower $\pi$-$\pi^*$ transition energy as compared to dfppy. This behavior is in sharp contrast with that observed for the heteroleptic Ir$^{III}$ complexes [Ir(dfppy)$_{3-x}$(ppy)$_x$] ($x$ =1, 2), whose emission energies are intermediate between those of the corresponding homoleptic complexes [Ir(dfppy)$_3$] and [Ir(ppy)$_3$], and shift gradually with the value of $x$.[19] Reasonably, the greater MLCT contribution to the emitting state in the Ir$^{III}$ complexes means that their emission energy is easily affected by the electronic properties of all of the ligands, while the primarily $^3$LC emission of the Pt$^{IV}$ derivatives should be less affected by the ligands that do not participate in the emission.

Unlike *fac*-**3ab**, complex *mer*-**3ab** is only weakly emissive in $CH_2Cl_2$ solution at 298 K ($\Phi$ < 0.01). The corresponding excitation spectrum practically coincides with the absorption spectrum of *fac*-**3ab**, which means that the registered emission arises mostly from small amounts of this intensely emissive isomer produced upon irradiation. Therefore, reliable room-temperature emission data for *mer*-**3ab** in solution could not be obtained. We have previously observed the same behavior in homoleptic *mer* isomers of tris-cyclometalated Pt$^{IV}$ complexes and attributed it to a thermally accessible ligand-to-metal charge-transfer (LMCT) excited state, which would provide a very effective nonradiative deactivation and be also responsible for the photoisomerization.[14]

**Table 3.** Emission data of complexes **3**.

| | 298 K[a] | | | | 77 K[b] |
|---|---|---|---|---|---|
| Complex | $\lambda_{em}$ [nm][c] ($\tau$ [μs])[d] | $\Phi$[e] | $k_r \times 10^{-3}$ [s$^{-1}$][f] | $k_{nr} \times 10^{-3}$ [s$^{-1}$][g] | $\lambda_{em}$ [nm][c] ($\tau$ [μs])[d] |
| *fac*-**3a**[i] | 436 (319) | 0.44 | 1.38 | 1.75 | 432 (636) |
| *fac*-**3b**[i] | 446 (216) | 0.49 | 2.27 | 2.37 | 443 (412) |
| *fac*-**3ab** | 447 (183) | 0.43 | 2.35 | 3.12 | 442 (465) |
| *mer*-**3ab** | — | — | — | — | 443 (766) |
| *mer*-**3ac** | 512 (108) | 0.046 | 0.43 | 8.81 | 507 (756) |
| *mer*-**3ad** | 416,[h] | 0.020 | — | — | 391,[h] |
| | 570 (41.5) | | | | 552 (156) |
| *mer*-**3bc** | 512 (113) | 0.072 | 0.64 | 8.21 | 506 (694) |
| *mer*-**3bd** | 570 (47.3) | 0.025 | 0.53 | 20.6 | 391,[h] |
| | | | | | 551 (165) |

[a] In $CH_2Cl_2$. [b] In frozen PrCN glass. [c] Highest-energy emission peak(s). [d] Emission lifetime. [e] Absolute quantum yield. [f] Radiative rate constant, $k_r = \Phi/\tau$. [g] Nonradiative rate constant, $k_{nr} = (1 - \Phi)/\tau$. [h] Fluorescence ($\tau$ < 0.2 ns). [i] Data from ref. [14].

The emissions of the heteroleptic complexes containing the thpy or piq ligand in $CH_2Cl_2$ at 298 K are appreciably more intense ($\Phi$ = 0.02–0.07) as compared to *mer*-**3ab**. In these cases, the excitation spectra faithfully reproduce the corresponding absorption profiles, which demonstrates that the observed emissions do not arise from possible impurities or from photodecomposition products. At 77 K, hypsochromic shifts between 200 and 600 cm$^{-1}$ relative to the room-temperature emissions are observed, which may be caused by a small rigidochromic effect. The emissions of the two thpy complexes *mer*-**3ac** and *mer*-**3bc** are identical (Figure 4) and of a lower energy (yellow) relative to the ppy-based emitters, which indicates that they arise from electronic transitions mainly localized on the thpy ligand and that the dfppy of ppy ligands have a negligible influence on the emission energy. The piq derivatives *mer*-**3ad** and *mer*-**3bd** also show identical phosphorescent emissions (Figure 4), but in the orange region, which can be ascribed to a transition within the piq ligand; however, these complexes exhibit an additional emission band at a higher energy, which is observable at 298 K for *mer*-**3ad** and for both complexes at 77 K. This secondary band can be ascribed to fluorescent emission in view of its small Stokes shift and very short lifetime (<0.2 ns), and the fact that no quenching was observed upon exposure to air. The excitation spectra registered at the fluorescence emission maximum are identical to

the absorption spectra and the relative intensities of the fluorescence and phosphorescence emissions are not sensitive to concentration changes in the range from $10^{-6}$ to $10^{-4}$ M, which rules out the possibility that aggregation effects or excimer formation could be responsible for the observed dual emission (see the Supporting Information for details). Dual phosphorescent/fluorescent emissions have been previously reported for other transition metal complexes that exhibit primarily LC emitting states.[6b, 8b, 20] In these systems, the SOC effects induced by the metal are less effective and fluorescence becomes competitive against the population of triplet states. Reasonably, the influence of the metal in the excited state of *mer*-**3ad** and *mer*-**3bd** must be significantly lower than in the thpy- or ppy-based emitters, because of the more extended π-system of the piq ligand.

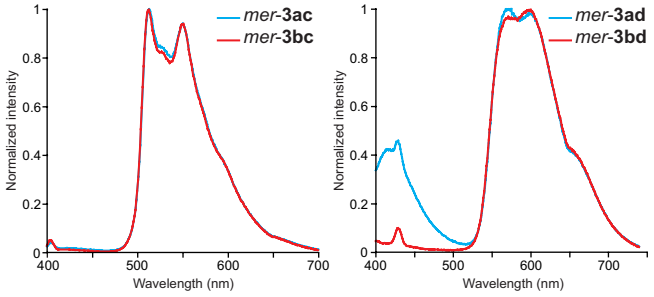


**Figure 4**. Emission spectra thpy-centered emitters (left) and piq-centered emitters (right) in $CH_2Cl_2$ at 298 K.

The radiative ($k_r$) and nonradiative ($k_{nr}$) rate constants at 298 K for the heteroleptic complexes (except *mer*-**3ab** and *mer*-**3ad**) were calculated according to the relationships $k_r = \Phi/\tau$ and $k_{nr} = (1 - \Phi)/\tau$, assuming that the emitting state is formed with unit efficiency upon excitation (Table 3). The $k_r$ and $k_{nr}$ values found for *fac*-**3ab** are similar to those of the homoleptic *fac* complexes. Notably, the *fac* geometry leads to very low $k_{nr}$ values, which implies that, in contrast to the corresponding *mer* isomers, nonradiative deactivation via higher-lying LMCT states might be negligible. Even though the heteroleptic thpy and piq derivatives here described have a *mer* configuration, they undergo much less nonradiative deactivation than *mer*-**3ab** or the previously reported homoleptic *mer* isomers;[14] clearly, the deactivating excited states are less accessible in these derivatives because the emitting states lie at lower energies. Moreover, the fact that the $k_{nr}$ values increase as the emission energy decreases suggests that nonradiative deactivation in both the *fac* isomers and the heteroleptic *mer* complexes could take place mainly through vibrational coupling to the ground state. This deactivation mechanism often conforms to the so-called energy gap law (EGL), which predicts an exponential increase of $k_{nr}$ with decreasing energy gap between the emitting excited state and the ground state.[21] A plot of $\ln k_{nr}$ *vs.* the emission energy ($E_{em}$) gives in fact a very good linear correlation ($R$ = 0.99; Figure 5), which confirms that the nonradiative decay at room temperature of the emitters here described and the previously reported homoleptic complexes *fac*-**3a** and **b** follows the EGL. Finally, it is noteworthy that the heteroleptic *mer* derivatives display significantly lower $k_r$ values as compared to the *fac* ones, which suggests that the *fac* geometry facilitates a higher metal orbital involvement in the emitting state.

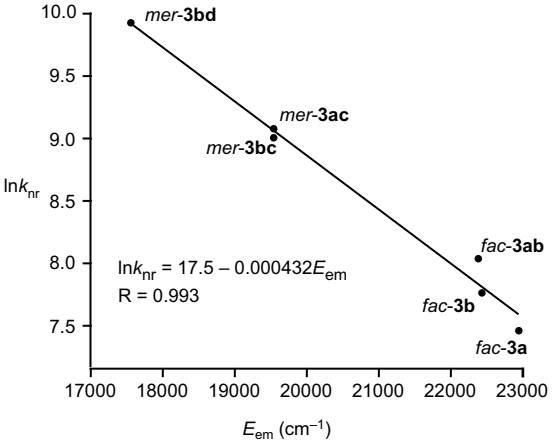


**Figure 5**. Plot of $\ln k_{nr}$ *vs.* the emission energy of tris-cyclometalated $Pt^{IV}$ complexes.

## Electrochemistry

The electrochemical properties of the new complexes were investigated using cyclic voltammetry in MeCN solution. For comparison purposes, the cyclic voltammograms of the homoleptic derivatives *mer*-**3a**,**3b** have been also registered, and those of *fac*-**3a**,**3b**[14] have been newly measured to cover the full solvent window (from 2.2 to –2.7 V *vs.* SCE). The potentials of the most important redox processes and HOMO/LUMO energy estimations are given in Table 4. Selected cyclic voltammograms are shown in Figure 6. The complete set of voltammograms is presented in the Supporting Information.

An irreversible oxidation peak was observed in the range from 1.72 to 1.97 V *vs.* SCE, except for *fac*-**3b** and the dfppy derivatives. It is noteworthy that the *mer* configuration leads to a higher HOMO energy relative to the *fac*, since the oxidation of *mer*-**3b** can be observed at +1.85 V *vs.* SCE while that of *fac*-**3b** falls beyond the solvent discharge limit.[14] Comparisons between *mer* isomers that share either the bis-cyclometalated unit containing the mutually trans nitrogens or the third ligand, reveal that the oxidation potential is affected by all of the cyclometalating ligands. Thus, for the series with the $Pt(ppy)_2$ subunit, the potential of the oxidation peak decreases as the third ligand is varied in the sequence ppy > piq > thpy, that is, as its electron-donating ability increases. The oxidation wave occurs at higher potentials for the $Pt(dfppy)_2$ series because of the lower electron-donating ability of the dfppy ligands and falls outside the solvent window except for complexes that contain piq or thpy as the third ligand. These data are consistent with primarily ligand-centered oxidations and indicate that the HOMO energy is affected by the three cyclometalating ligands.

**Table 4.** Electrochemical data[a] and HOMO/LUMO energy estimations[b] for complexes **3**.

| Complex | $E_{pa}$ [c] | $E_{pc}$ [d] | $E_{1/2}$ [e] | $E_{HOMO}$ | $E_{LUMO}$ | $\Delta E_{HOMO-LUMO}$ |
|---|---|---|---|---|---|---|
| *mer*-**3a** | —[f] | –1.25 | –2.25 | — | –3.55 | — |

| | | | | | | |
|---|---|---|---|---|---|---|
| *fac*-**3a** | —[f] | –1.60 | –2.25 | — | –3.19 | — |
| *mer*-**3b** | 1.85 | –1.50 | –2.39 | –6.42 | –3.27 | 3.15 |
| *fac*-**3b** | —[f] | –1.80 | –2.39 | — | –2.71 | — |
| *mer*-**3ab** | —[f] | –1.32 | –2.31 | — | –3.45 | — |
| *fac*-**3ab** | —[f] | –1.64 | –2.30 | — | –3.14 | — |
| *mer*-**3ac** | 1.84 | –1.29 | –2.26 | –6.40 | –3.51 | 2.89 |
| *mer*-**3ad** | 1.97 | –1.31 | –2.22 | –6.52 | –3.47 | 3.05 |
| *mer*-**3bc** | 1.72 | –1.50 | –2.36 | –6.29 | –3.27 | 3.02 |
| *mer*-**3bd** | 1.82 | –1.45 | —[g] | –6.38 | –3.33 | 3.05 |

[a] In V relative to SCE, measured in 0.1 M $(Bu_4N)PF_6$ anhydrous MeCN solution at 100 mV $s^{-1}$. [b] In eV; estimated from the onset values of the oxidation and reduction waves referenced against $Fc^+/Fc$ (0.40 V vs. SCE in MeCN), using a formal potential of 5.1 eV for the $Fc^+/Fc$ couple in the Fermi scale.[22] [c] Irreversible anodic peak potential. [d] First irreversible cathodic peak potential. [e] For the reversible process. [f] Outside solvent window. [g] Could not be determined accurately.

The cyclic voltammograms of the *mer* complexes show several reduction processes. The first one gives rise to an irreversible wave at around –1.30 for the $[Pt(dfppy)_2(C'^N')]^+$ derivatives or –1.50 V *vs.* SCE for the $[Pt(ppy)_2(C'^N')]^+$ derivatives, indicating that the energy of the LUMO is mainly dictated by the $Pt(C^N)_2$ subunit with the mutually trans nitrogens. The observed potential for the reduction of complex *fac*-**3ab** is very similar to that of the homoleptic complex *fac*-**3a**, indicating that the LUMO is mainly located on the dfppy ligands. At more negative potentials, other irreversible reduction processes can be distinguished in most cases (Figure 6). In addition to them, a reversible wave with $E_{1/2}$ in the range from –2.22 to –2.39 V *vs.* SCE is observed in all cases, which corresponds to the reduction and reoxidation of one of the species produced during the previous irreversible reductions. Most probably, this species is a neutral bis-cyclometalated $Pt^{II}$ complex *cis*-$[Pt(C^N)_2]$ or *cis*-$[Pt(C^N)(C'^N')]$, since the $E_{1/2}$ values are close to that previously reported for *cis*-$[Pt(ppy)_2]$ (–2.19 V *vs.* SCE).[23]

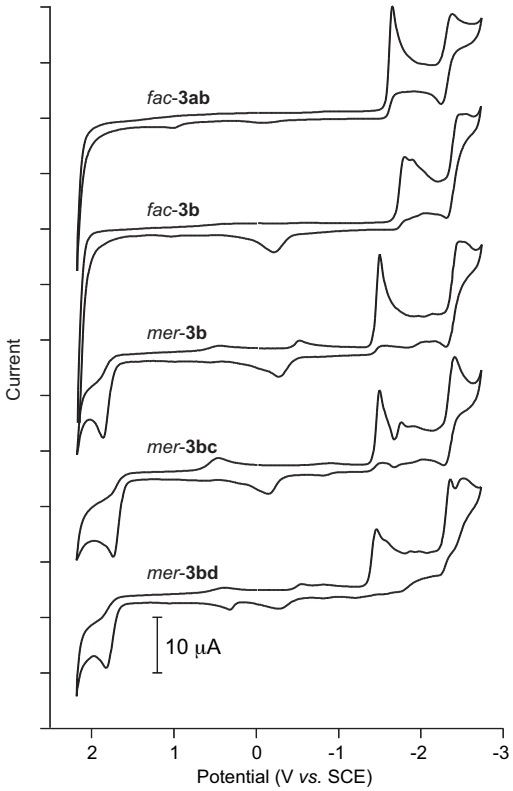


**Figure 6**. Cyclic voltammograms of *fac*-**3ab**, *fac/mer*-**3b**, *mer*-**3bc** and *mer*-**3bd** in MeCN at 100 mV $s^{-1}$.

## Computational calculations

In order to get a better understanding of the photophysical properties of tris-cyclometalated $Pt^{IV}$ complexes, we have carried out DFT and TD-DFT calculations for *mer*-**3bc** and *mer*-**3bd**, as well as the previously reported homoleptic complexes *fac/mer*-**3b**. The bond distances and angles of the optimized geometries are in good agreement with the expected values in view of the crystal structures of *mer*-**3ab** and *mer*-**3ac** (see the Supporting Information for details). A diagram comparing the frontier orbital energies of the four calculated cations is represented in Figure 7 and isodensity surfaces of these molecular orbitals are depicted in Figure 8. The compositions of the molecular orbitals from atomic orbital contributions are given in the Supporting Information.

The strictly $C_3$-symmetrical geometry of the cation of *fac*-**3b** in the gas phase leads to orbital degeneracy and very compact sets of frontier orbitals. The HOMO of A symmetry is equally distributed over the three ppy ligands (31% each, mainly from $\pi$ orbitals of the phenyl rings) and has around 6% of metal orbital contribution. At slightly lower energies are two degenerate orbitals of E symmetry, also with the largest contributions from the phenyl rings but less metal character (5%). There are three close-lying LUMOs, one of A symmetry uniformly distributed over the three ppy ligands and a pair of degenerate E orbitals, all of them with the largest contributions from $\pi^*$ orbitals of the pyridyl rings and little metal character. A pair of degenerate unoccupied MOs with a large metal orbital contribution (35%) lie at significantly higher energies.

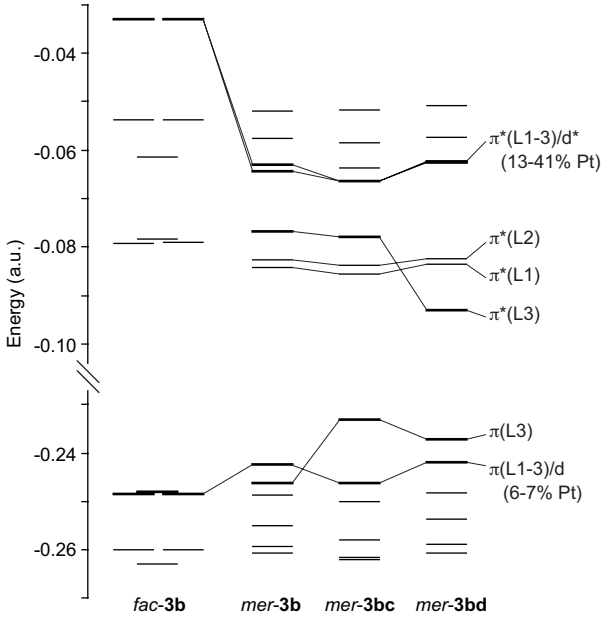


**Figure 7**. Orbital energy diagrams from DFT calculations for *fac*/*mer*-**3b**, *mer*-**3bc** and *mer*-**3bd** in $CH_2Cl_2$ solution. See Scheme 2 for ligand numbering in the *mer* complexes.

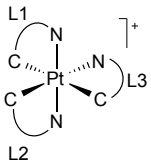


| | L1, L2 | L3 |
|---|---|---|
| *mer*-**3b** | ppy | ppy |
| *mer*-**3bc** | ppy | thpy |
| *mer*-**3bd** | ppy | piq |

**Scheme 2**. Ligand numbering for the calculated *mer* complexes.

The lower symmetry of the *mer* isomers (point group $C_1$) results in a less compact distribution of frontier orbitals. In all the three cases, there is an occupied orbital with around 7% of metal contribution (having an important π character across the C–Pt–C axis) and varying contributions from the three cyclometalating ligands (15–56%, mainly from π orbitals of the phenylic rings), which is the HOMO in *mer*-**3b**, whereas it becomes the HOMO–1 in the heteroleptic derivatives *mer*-**3bc** and *mer*-**3bd**. The HOMO in the latter two complexes is a π orbital of the thpy or piq ligand and has very little metal character. In line with the electrochemical data, the predicted HOMO energy for *mer*-**3b** is higher than that of its *fac* counterpart, and the thpy complex *mer*-**3bc** displays the highest HOMO energy among the calculated *mer* complexes. The first three LUMOs in the three *mer* complexes are π* orbitals mainly localized on the pyridyl or isoquinolyl system of each of the cyclometalating ligands (Figure 8). There is also an unoccupied molecular orbital with up to 41% of metal orbital contribution (having $z^2$ character along the N–Pt–N axis) at considerably lower energies as compared to those of *fac*-**3b**, which indicates that LMCT transitions should occur at significantly lower energies in the *mer* complexes.

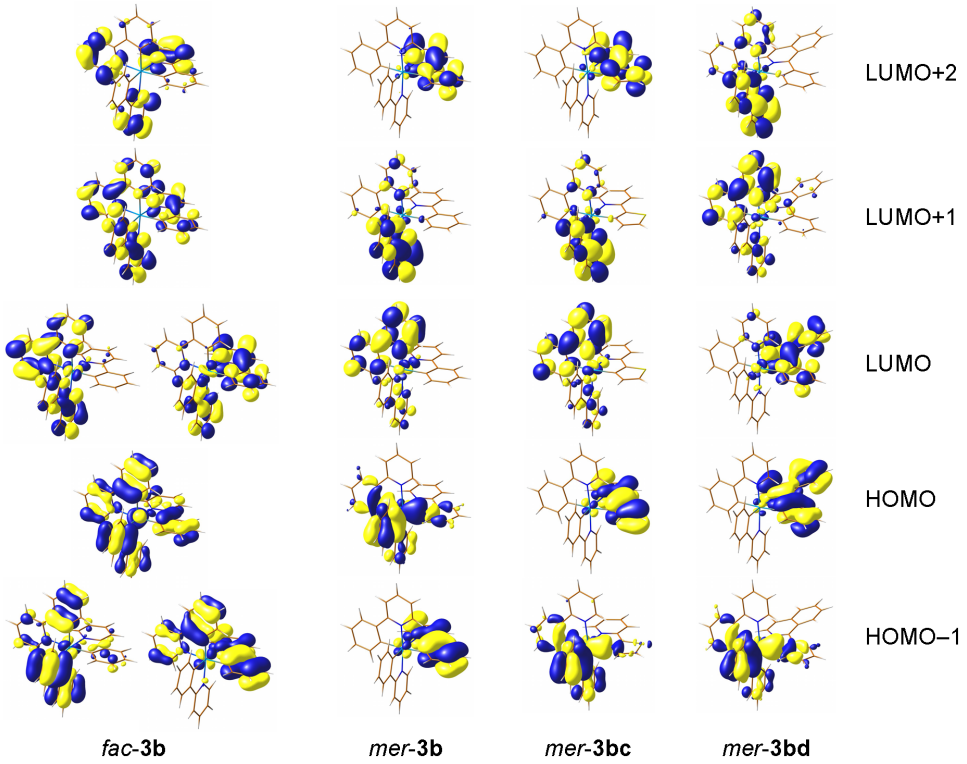


**Figure 8**. Selected molecular orbital isosurfaces (0.03 e·bohr$^{-3}$) for *fac*/*mer*-**3b**, *mer*-**3bc** and *mer*-**3bd**.

Excitation energies at the ground state geometry were calculated by TD-DFT in $CH_2Cl_2$ solution. The data for the singlets with the highest oscillator strengths and the first three triplets in $CH_2Cl_2$ are listed in Tables 5-7. A more extensive listing of excited states is given in the Supporting Information. The calculated singlet excitations are in good qualitative agreement with the experimental absorption spectra (Figure 9). In general, the most intense singlet excitations correspond to transitions largely of LC character. In the cases of the *mer* complexes, many of these excitations have some ligand-to-ligand charge-transfer (LLCT) character. As expected, the lowest-energy singlet excitation in the heteroleptic complexes *mer*-**3bc** and *mer*-**3bd** is localized within the thpy or piq ligand, respectively; it is also noteworthy that transitions of main LLCT character become more important for these derivatives, which is reasonable in view of the very different electronic properties of the ppy and thpy or piq ligands.

The character of charge transfer between the metal and the ligand (%CT) for each excited state was estimated from the percentage of metal orbital contribution (%M) to the orbitals involved in each of the participating monoexcitations, as shown in Equation 1, where $C(i\rightarrow j)$ are the coefficients of each of the $i\rightarrow j$ monoexcitations.[24]

$$\%CT=\sum_{i,j}[C(i\rightarrow j)]^2(\%M_i-\%M_j) \quad (1)$$

Positive %CT values indicate net metal-to-ligand charge transfer (MLCT) contributions, while negative values indicate ligand-to-metal charge transfer (LMCT) (Tables 5 and 6). In spite of the fact that most of the estimated %CT values are very low and appear to bear little significance, there are clear differences between *fac*-**3b** and the *mer* complexes. The lowest-energy LC singlet excitations in *fac*-**3b** have a net MLCT contribution (up to 4%), while transitions with LMCT character have generally much lower oscillator strengths and the most intense is predicted at 5.06 eV ($S_{39}$, 245 nm). In contrast, many of the singlet absorptions in the *mer* complexes have some LMCT character, which is explained by the lower energies of the unoccupied molecular orbitals with a high metal orbital involvement. More specifically, absorptions of LMCT character higher than 10% and appreciable oscillator strengths are predicted to occur at around 4.5 (*mer*-**3b** and *mer*-**3bd**) or 4.1 eV (*mer*-**3bc**) and at higher energies. Therefore, the presence of low-lying LMCT states is a common characteristic of the *mer* isomers. These states may trigger the photoisomerization of *mer*-**3b** and *mer*-**3ab**, as well as the photodecomposition of the heteroleptic thpy and piq derivatives, because they involve the population of antibonding d orbitals, which may lead to bond dissociation and/or reduction of the metal center.

**Table 5.** Selected vertical singlet excitations of *fac/mer*-**3b** from TD-DFT calculations at the $S_0$ geometry in $CH_2Cl_2$.

| compd | state | main monoexcitations[a] | ΔE/eV | λ/nm | oscillator strength | main character | metal %CT |
|---|---|---|---|---|---|---|---|
| *fac*-**3b** | $S_1$ | H→L (86%) | 3.98 | 311 | 0.038 | LC | 1.7 |
| | $S_2$ | H→L (86%) | 3.98 | 311 | 0.040 | LC | 1.7 |
| | $S_3$ | H-1→L (72%) | 4.00 | 310 | 0.237 | LC | 1.0 |
| | $S_{10}$ | H-2→L (58%) | 4.29 | 289 | 0.085 | LC | 1.1 |
| | $S_{11}$ | H-2→L (57%) | 4.29 | 289 | 0.085 | LC | 1.3 |
| | $S_{12}$ | H-2→L (80%) | 4.31 | 288 | 0.081 | LC | 1.2 |
| | $S_{19}$ | H→L+2 (70%) | 4.55 | 273 | 0.141 | LC | 4.0 |
| | $S_{24}$ | H-1→L+3 (89%) | 4.73 | 262 | 0.112 | LC | 1.8 |
| | $S_{39}$ | H-1→L+4 (64%) | 5.06 | 245 | 0.046 | LC/LMCT | –20.4 |
| *mer*-**3b** | $S_2$ | H→L+1 (88%) | 3.68 | 337 | 0.115 | LC | 4.5 |
| | $S_9$ | H-1→L+2 (78%) | 4.04 | 307 | 0.171 | LC | - |
| | $S_{12}$ | H-3→L+1 (72%) | 4.12 | 301 | 0.095 | LC | - |
| | $S_{14}$ | H-5→L (44%) H-1→L+3 (19%) | 4.16 | 298 | 0.051 | LC/LLCT/ LMCT | –7.5 |
| | $S_{20}$ | H-4→L+2 (29%) H-3→L+2 (49%) | 4.28 | 290 | 0.039 | LC/LLCT | –1.8 |
| | $S_{25}$ | H-6→L (32%) H-1→L+3 (28%) | 4.43 | 280 | 0.050 | LC/LLCT | –4.3 |
| | $S_{28}$ | H-2→L+3 (51%) H-2→L+4 (20%) | 4.49 | 276 | 0.066 | LC/LLCT/ LMCT | –11.1 |
| | $S_{34}$ | H-3→L+3 (56%) H-3→L+4 (23%) | 4.68 | 265 | 0.056 | LC/LLCT/ LMCT | –12.5 |

[a] H and L stand for Highest Occupied Molecular Orbital (HOMO) and Lowest Unoccupied Molecular Orbital (LUMO), respectively.

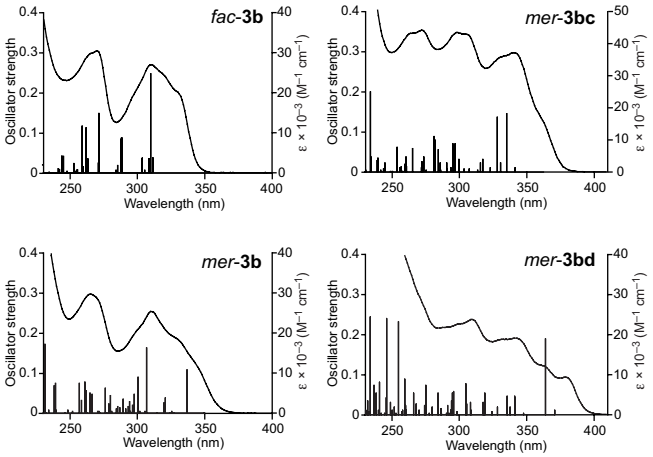


**Figure 9**. Calculated stick absorption spectra of *fac*/*mer*-**3b**, *mer*-**3bc** and *mer*-**3bd** in $CH_2Cl_2$ compared with the experimental spectra.

**Table 6.** Selected vertical singlet excitations of *mer*-**3bc** and *mer*-**3bd** from TD-DFT calculations at the $S_0$ geometry in $CH_2Cl_2$.

| compd | state | main monoexcitations[a] | ΔE/ eV | λ/nm | oscillator strength | main character | metal %CT |
|---|---|---|---|---|---|---|---|
| *mer*-**3bc** | $S_4$ | H→L+2 (69%) | 3.70 | 336 | 0.149 | LC(thpy) | –3.8 |
| | $S_6$ | H-1→L+1 (69%) | 3.77 | 329 | 0.141 | LC(ppy)/ LLCT | 2.4 |
| | $S_8$ | H-1→L+2 (53%) H-1→L+3 (23%) | 3.90 | 318 | 0.034 | LLCT | –5.2 |
| | $S_{14}$ | H-5→ L (25%) H-2→L+2 (29%) H-2→L+3 (28%) | 4.13 | 300 | 0.033 | LC(ppy)/ LLCT/LM CT | –11.2 |
| | $S_{15}$ | H-3→L+1 (38%) H→ L+5 (50%) | 4.17 | 297 | 0.074 | LC(ppy)/ LLCT | - |

| | | | | | | | |
|---|---|---|---|---|---|---|---|
| | $S_{17}$ | H-5→L (49%)<br>H-2→L+3 (15%) | 4.19 | 296 | 0.075 | LC(ppy)<br>/LMCT | –7.2 |
| | $S_{23}$ | H-3→L+2 (12%)<br>H-3→L+3 (50%)<br>H→L+6 (10%) | 4.35 | 285 | 0.059 | LLCT/LM<br>CT | –21.3 |
| | $S_{24}$ | H→L+6 (69%) | 4.39 | 282 | 0.083 | LC (thpy) | –3.7 |
| | $S_{25}$ | H-4→L+2 (74%) | 4.40 | 282 | 0.090 | LC (thpy) | 1.0 |
| *mer*-**3bd** | $S_2$ | H→L (78%) | 3.42 | 363 | 0.183 | LC(piq) | –1.0 |
| | $S_5$ | H-2→L (71%) | 3.65 | 340 | 0.045 | LLCT | 1.2 |
| | $S_7$ | H-1→L+2 (49%)<br>H→L+2 (31%) | 3.71 | 335 | 0.046 | LC(ppy)/<br>LLCT | 2.3 |
| | $S_{10}$ | H-2→L+1 (45%)<br>H-1→L+3 (15%)<br>H-1→L+4 (19%) | 3.90 | 318 | 0.053 | LC(ppy) | –3.6 |
| | $S_{16}$ | H-3→L+2 (86%) | 4.08 | 304 | 0.077 | LC(ppy)<br>/LLCT | 1.2 |
| | $S_{19}$ | H-4→L+1 (64%)<br>H-4→L+2 (17%) | 4.21 | 295 | 0.058 | LLCT | - |
| | $S_{21}$ | H-5→L+1 (57%) | 4.23 | 293 | 0.037 | LC (ppy) | –1.0 |
| | $S_{28}$ | H-8→L (21%)<br>H→L+6 (38%) | 4.38 | 283 | 0.052 | LC (piq) | |
| | $S_{32}$ | H-2→L+3 (29%)<br>H-2→L+4 (49%) | 4.52 | 274 | 0.073 | LC/LLCT/<br>LMCT | –14.8 |

[a] H and L stand for Highest Occupied Molecular Orbital (HOMO) and Lowest Unoccupied Molecular Orbital (LUMO), respectively.

The TD-DFT calculations at the $S_0$ geometry in $CH_2Cl_2$ predict the three lowest triplet states of *fac*-**3b** to be nearly degenerate at around 2.96 eV (419 nm) above the ground state (Table 7). An analysis of the one-electron excitations that contribute to these transitions reveals that they are largely centered on the ligands, with a very small MLCT contribution. The three lowest triplets of *mer*-**3b** are also nearly degenerate and have very similar energies to those of the *fac* isomer. However, each of these excitations is confined within a different cyclometalating ligand. A similar situation is found in the heteroleptic complexes *mer*-**3bc** and *mer*-**3bd**, although, as expected, the triplet excitation within the thpy or piq ligand is significantly lower in energy than those within the ppy ligands. Notably, the three lowest triplet excitations in the *mer* complexes differ in the estimated %CT contribution, which can be insignificant or even have a certain LMCT character. Moreover, an inspection of the estimated %CT values of higher-lying triplets reveals that in the cases of the *mer* complexes there are several states of significant LMCT character (greater than 10%) at relatively low energies (3.6–4.2 eV; Figure 10), while in the case of the *fac*-**3b** no such states can be found below 4.6 eV (see the Supporting Information). The presence of these states may explain the effective nonradiative deactivation of *mer*-**3b** at room temperature, since they are close in energy to the emitting (lowest) triplet state and might be thermally populated. The lower energy of the emitting state in *mer*-**3bc** or *mer*-**3bd** implies that the thermal population of LMCT states should be less favored and is consistent with our observation that the main contribution to nonradiative deactivation in these derivatives is vibrational coupling to the ground state.

**Table 7.** Lowest-energy vertical triplet excitations of *fac*-**3b**, *mer*-**3b**, *mer*-**3bc** and *mer*-**3bd** from TD-DFT calculations at the $S_0$ geometry in $CH_2Cl_2$.

| compd | state | main monoexcitations | $\Delta E$/eV | $\lambda$/nm | main character | metal %CT |
|---|---|---|---|---|---|---|
| *fac*-**3b** | $T_1$ | H–1→L (25%)<br>H–1→L+1 (24%)<br>H→L (23%) | 2.96 | 419 | LC | 1.3 |
| | $T_2$ | H–1→L (19%)<br>H–1→L+1 (27%)<br>H→L (25%) | 2.96 | 419 | LC | 1.5 |
| | $T_3$ | H–1→L (47%)<br>H→L+1 (27%) | 2.97 | 418 | LC | 1.5 |
| *mer*-**3b** | $T_1$ | H–2→L (64%) | 2.91 | 426 | LC (L1)[b] | –1.0 |
| | $T_2$ | H–3→L+1(38%)<br>H→L+1 (19%) | 2.96 | 419 | LC (L2)[b] | 1.6 |
| | $T_3$ | H–1→L+2 (67%) | 2.96 | 419 | LC (L3)[b] | 1.0 |
| *mer*-**3bc** | $T_1$ | H→L+2 (86%) | 2.52 | 491 | LC (thpy) | 0 |
| | $T_2$ | H–2→L (62%) | 2.91 | 426 | LC (ppy) | –1.8 |
| | $T_3$ | H–3→L+1 (34%)<br>H–1→L+1 (31%) | 2.96 | 419 | LC (ppy) | 2.2 |
| *mer*-**3bd** | $T_1$ | H→L(83%) | 2.37 | 524 | LC (piq) | –1.8 |
| | $T_2$ | H–2→L+1 (56%)<br>H–2→L+2 (19%) | 2.91 | 426 | LC (ppy) | 1.0 |
| | $T_3$ | H–4→L+2 (11%)<br>H–3→L+2 (36%)<br>H–1→L+2 (18%) | 2.96 | 419 | LC (ppy) | 2.1 |

[a] H and L stand for Highest Occupied Molecular Orbital (HOMO) and Lowest Unoccupied Molecular Orbital (LUMO), respectively. [b] See Scheme 2 for ligand numbering.

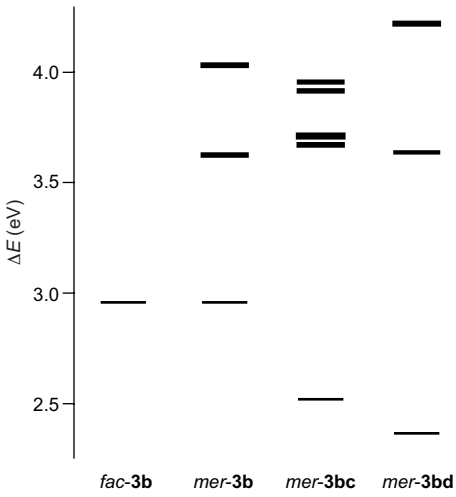


**Figure 10.** Simplified excited-state energy diagram showing the lowest-lying triplet (thin lines) and the triplet states with a LMCT character greater than 10% (thick lines) for *fac/mer*-**3b**, *mer*-**3bc** and *mer*-**3bd** from TD-DFT calculations at the ground-state geometry.

To gain further insight into the emitting behavior of tris-cyclometalated $Pt^{IV}$ complexes, the geometry of the lowest triplet

excited state in $CH_2Cl_2$ solution was optimized for the four calculated cations. The calculated electronic energies with respect to the ground state (adiabatic energy differences) are 2.84 (*fac/mer*-**3b**), 2.36 (*mer*-**3bc**) or 2.22 eV (*mer*-**3bd**), and correctly follow the trend of the observed emission energies. The modifications on going form the $S_0$ geometry to the relaxed lowest-energy triplet geometry affect only to one of the cyclometalating ligands, which, in the cases of the heteroleptic derivatives is the thpy or piq ligand, while in *mer*-**3b** is the ppy ligand in the analogous position, that is, the one with a nitrogen in *trans* to a carbon atom (L3 in Scheme 2). The affected ligand is pulled toward the metal, as a result of a slight shortening of the Pt–N bond by about 0.02 Å in all cases, and also the Pt–C bond in *fac*/*mer*-**3b** and *mer*-**3bc** by about 0.01 Å. In addition, the bond distances within the ligand undergo significant variations, which are consistent with the population of a $\pi^*$ orbital (see the Supplementary Information for details). The spin density distribution (Figure 11) matches in all cases the topology of a $\pi$-$\pi^*$ excitation localized exclusively on the ligand that undergoes the geometry modifications. This is consistent with the fact that the emission spectra of complexes that share the ligand of lowest $\pi$-$\pi^*$ transition energy are identical, while the remaining ligands do not have an observable influence on the emission energies. The spin density on the platinum atom is very low, although noticeably higher for *fac*-**3b** (0.018) than for the *mer* complexes (range 0.007–0.009). Therefore, the calculations predict a higher metal orbital involvement in the excited state for the *fac* geometry, which should lead to higher radiative rate constants.

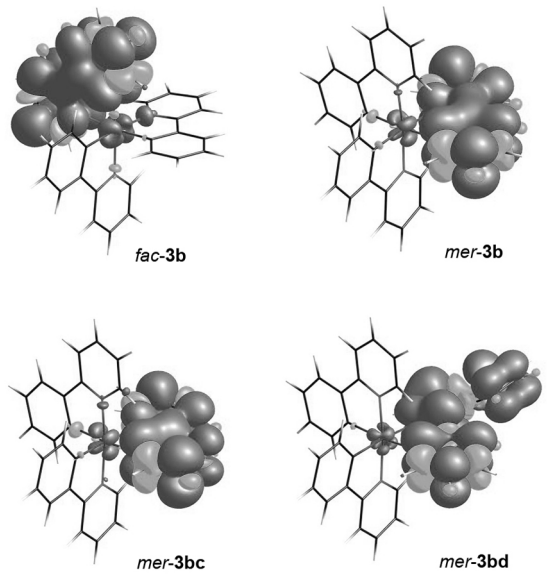


**Figure 11**. Spin density distributions (0.001 e·bohr$^{-3}$) for the lowest triplet excited state in complexes *fac/mer*-**3b**, *mer*-**3bc** and *mer*-**3bd**.

## Conclusion

Heteroleptic tris-cyclometalated $Pt^{IV}$ complexes containing one cyclometalating ligand of a relatively low $\pi$-$\pi^*$ transition energy, *mer*-[Pt(C^N)$_2$(C'^N')]OTf (C^N = dfppy or ppy and C'^N' = thpy or piq) were prepared in moderate to good yields. In addition, the complex *mer*-[Pt(dfppy)$_2$(ppy)]OTf was obtained and photoisomerized to its *fac* counterpart.

With the exception of *mer*-[Pt(dfppy)$_2$(ppy)]OTf, the heteroleptic complexes here described display long-lived luminescence in fluid solution at room temperature, with emission colors that range from blue to orange. The characteristics of the emissions are compatible with triplet emitting states involving electronic transitions almost exclusively localized on the ligand with the lowest $\pi$-$\pi^*$ transition energy, which is further substantiated by DFT calculations. The involvement of the metal orbitals in the excited states is very low, but it is sufficient to promote a very effective intersystem crossing to the emitting triplet state that precludes fluorescence emission in most cases.

Complexes with a *fac* configuration exhibit considerably higher emission quantum yields, associated with higher radiative rates and lower nonradiative rates, as compared to the *mer* isomers. A higher metal orbital involvement in the excited state may explain the higher radiative rate constants observed for the *fac* isomers, as predicted by our calculations. On the other hand, the theoretical study supports our previous assumption that deactivating excited states of LMCT character must be much higher in energy in the *fac* isomers, while they may become thermally accessible from the emitting state in the *mer* isomers. Nevertheless, the heteroleptic *mer* complexes containing thpy or piq as the chromophoric ligand do not undergo such deactivation mechanism because their emitting states lie at relatively low energies. In fact, our study demonstrates that the main contribution to nonradiative deactivation in these derivatives as well as in the *fac* complexes originates from vibrational coupling to the ground state.

The present work provides a first approximation to the development of tris-cyclometalated $Pt^{IV}$ complexes that exhibit relatively low absorption and emission energies as well as long radiative lifetimes. In addition, it constitutes a fundamental study on the factors that govern the excited-state properties of this class of compounds, which will facilitate the rational design of new complexes of this class with improved properties. Further work in our laboratory will focus on the development of alternative synthetic routes to color-tunable tris-cyclometalated $Pt^{IV}$ complexes and the study of their applications.

## Experimental Section

### General considerations and materials

Unless otherwise noted, preparations were carried out under atmospheric conditions. The compounds $PhICl_2$,[25] **1a–d**,[26] and **2a** and **2b**[13c] were prepared following published procedures. Complexes **2c**, **2d** and **4d** were not previously reported and their synthesis and spectroscopic and analytical data are given in the Supporting Information. All other reagents were obtained from commercial sources and used without further purification. Synthesis grade solvents were obtained from commercial sources. NMR spectra were recorded on Bruker Avance 200, 300 or 400 spectrometers at 298 K. Chemical shifts are referred to residual signals of non-deuterated solvent. The number of solvation water molecules was calculated from the integral of the $^1$H NMR water signal, taking into account the water content of the solvent blank. Elemental analyses were carried out with Carlo Erba 1106 and LECO CHNS-932 microanalyzers. Photoisomerizations were carried out using a UV-Consulting Peschl photoreactor, model UV-RS-1, equipped with a 150 W medium-pressure mercury immersion UV lamp (TQ 150), a quartz cooling jacket, and a 400 mL reaction vessel with magnetic circulation pump.

**X-ray structure determinations**

Crystals of *mer*-**3ab**·2$Et_2O$ and *mer*-**3ac**·$Et_2O$ suitable for X-ray diffraction studies were obtained by the liquid-liquid diffusion method from $CH_2Cl_2$/$Et_2O$. Numerical details are presented in Table 8. The data were collected on Bruker D8 QUEST (*mer*-**3ab**) or Bruker SMART APEX CCD (*mer*-**3ac**) diffractometers using monochromated Mo-$K\alpha$ radiation in $\omega$-scan mode. The structures were solved by direct methods and refined anisotropically on $F^2$ using the program SHELXL-2013 (*mer*-**3ab**) or SHELXL-97 (*mer*-**3ac**) (G. M. Sheldrick, University of Göttingen).[27] Hydrogens were included using rigid methyl groups or a riding model. *Special features of refinement:* In *mer*-**3ab**·2$Et_2O$, one of the $Et_2O$ molecules is badly disordered and its hydrogens were not included in the refinement. In *mer*-**3ac**, there is a poorly resolved region of residual electron density that could not be adequately modeled and therefore the program SQUEEZE,[28] which is part of the PLATON system, was employed to remove mathematically the effects of the solvent. The void volume per cell was 549 $Å^3$, with a void electron count per cell of 145; this additional solvent was not taken into account when calculating derived parameters such as the formula weight, because its nature was uncertain. The triflate anion is disordered over two positions, *ca.* 64:36% (*mer*-**3ab**) or 55:45% (*mer*-**3ac**). CCDC 1014867 and CCDC 1014868 contain the supplementary crystallographic data for this paper. These data can be obtained free of charge from the Cambridge Crystallographic Data Centre via http://www.ccdc.cam.ac.uk/data_request/cif.

**Table 8.** Crystallographic Data for *mer*-**3ab**·2$Et_2O$ and *mer*-**3ac**·$Et_2O$.

| | *mer*-**3ab**·2$Et_2O$ | *mer*-**3ac**·$Et_2O$ |
|---|---|---|
| formula | $C_{42}H_{40}F_7N_3O_5PtS$ | $C_{36}H_{28}F_7N_3O_4PtS_2$ |
| $M_r$ [g $mol^{-1}$] | 1026.92 | 958.82 |
| $T$ [K] | 100(2) | 100(2) |
| $\lambda$ [Å] | 0.71073 | 0.71073 |
| crystal system | monoclinic | monoclinic |
| space group | $P2_1/c$ | $P2_1/c$ |
| $a$ [Å] | 10.2797(7) | 10.1139(7) |
| $b$ [Å] | 14.1860(10) | 13.8302(9) |
| $c$ [Å] | 27.7497(19) | 28.3028(18) |
| $\beta$ [°] | 94.589(2) | 95.479(2) |
| $V$ ($Å^3$) | 4033.7(5) | 3940.8(5) |
| $Z$ | 4 | 4 |
| $\rho_{calcd}$ [Mg $m^{-3}$] | 1.689 | 1.616 |
| $\mu$ [$mm^{-1}$] | 3.612 | 3.740 |
| R1[a] | 0.0351 | 0.0265 |
| wR2[b] | 0.0834 | 0.0619 |

[a] $R1 = \Sigma||F_o|-|F_c||/\Sigma|F_o|$ for reflections with $I > 2\sigma(I)$. [b] $wR2 = [\Sigma[w(F_o^2 - F_c^2)^2]/\Sigma[w(F_o^2)^2]^{0.5}$ for all reflections; $w^{-1} = \sigma^2(F^2) + (aP)^2 + bP$, where $P = (2F_c^2 + F_o^2)/3$ and $a$ and $b$ are constants set by the program.

**Photophysical characterization**

UV-vis absorption spectra were recorded on a Perkin-Elmer Lambda 750S spectrophotometer. Excitation and emission spectra were recorded on a Jobin Yvon Fluorolog 3-22 spectrofluorometer with a 450 W xenon lamp, double-grating monochromators, and a TBX-04 photomultiplier. Solution measurements were carried out in a right angle configuration using 10 mm quartz fluorescence cells or 5 mm quartz NMR tubes. For the low-temperature measurements, a liquid nitrogen Dewar with quartz windows was employed. Solutions of the samples were degassed by bubbling argon for 30 min. Lifetimes were measured using the Fluorolog's FL-1040 phosphorimeter accessory; the estimated uncertainty is ±10% or better. Emission quantum yields were measured using a Hamamatsu C11347 Absolute PL Quantum Yield Spectrometer; the estimated uncertainty is ±5% or better.

**Electrochemical characterization**

Cyclic voltammograms were registered with a potentiostat/galvanostat AUTOLAB-100 (Echo-Chemie, Utrecht), employing a three-electrode electrochemical cell equipped with a glassy carbon working electrode (Metrohm, 2 mm diameter), an Ag/AgCl/3 M KCl electrode reference, and a glassy carbon rod counter electrode. The measurements were carried out at 298 K under an argon atmosphere, using degassed 1 mM solutions of the complexes in extra-dry MeCN (Acros Organics) and 0.1 M $(Bu_4N)PF_6$ as the electrolyte. Prior to each experiment, the working electrode was polished with alumina slurry (0.05 μm) and rinsed with water and acetone. The electrodes were activated electrochemically in the background solution by means of several voltammetric cycles at 1 V $s^{-1}$ between –2.7 V and 2.2 V. At the end of each experiment, the reference electrode was checked against the ferrocene/ferricinium redox couple. Potentials are given *vs.* the standard calomel electrode (SCE).

**Synthesis of *mer*-[Pt(C^N)$_2$(C'^N')].**

The appropriate [Pt(C^N)$_2$Cl$_2$] precursor (0.22 mmol), Ag(OTf) (0.48 mmol), and the N'^C'H pro-ligand (0.88 mmol) were placed in a Carius tube and suspended in degassed 1,2-dichloroethane (15 mL) under a nitrogen atmosphere. The mixture was heated at 90 ºC for 2 days. After cooling to room temperature, $CH_2Cl_2$ (10 mL) was added and the suspension was filtered trough Celite. The filtrate was stirred vigorously with $Na_2CO_3$ and then filtered. The solvent was removed under reduced pressure and the remaining residue was purified by crystallization from $CH_2Cl_2$/$Et_2O$ (*mer*-**3ab**, **3ac**, and **3bc**) or by column chromatography on silica gel (*mer*-**3ad**, **3bd**) using a $CHCl_3$/MeOH mixture (9:1) as the eluent.

***mer*-3ab·0.5H$_2$O.** White solid. Yield: 73%. $^1$H NMR (300.1 MHz, $CD_3CN$): $\delta$ = 8.43 (m, 2 H), 8.32 (d, $J$(H,H) = 8.4 Hz, 1 H), 8.18-7.93 (m, 6 H), 7.67 (d with satellites, $J$(H,H) = 6.0, Hz, $J$(H,Pt) = 30.6 Hz, 1 H), 7.40-7.21 (m, 5 H), 6.99 (m, 2 H), 6.75 (d with satellites, $J$(H,H) = 7.4 Hz, $J$(H,Pt) = 20.6 Hz, 1 H), 6.06 (dd with satellites, $J$(H,H) = 6.7, 2.3 Hz, $J$(H,Pt) = 18.8 Hz, 1 H), 5.76 (dd with satellites, $J$(H,H) = 8.1, 2.2 Hz, $J$(H,Pt) = 37.8 Hz, 1 H); $^{13}$C{$^1$H} NMR (75.45 MHz, $CD_3CN$: $\delta$ = 168.0-160.4 (several multiplets; C), 151.4 ($J$(C,Pt) = 16 Hz; CH), 150.3 (CH), 148.2 (CH), 144.9 (C), 144.0 (CH), 143.2 (CH), 143.1 (CH), 133.9 (m; CH), 128.2-126.3 (m; CH), 123.7 ($J$(C,Pt) = 14 Hz; CH), 114.5 (m; CH), 111.7 (m; CH), 104.3-102.8 (m; CH); elemental analysis calcd (%) for $C_{34}H_{21}F_7N_3O_{3.5}PtS$: C 46.00, H 2.38, N 4.73, S 3.61; found: C 46.04, H 2.19, N 4.71, S 3.77.

***mer*-3ac·0.5H$_2$O.** Off-white solid. Yield: 86%. $^1$H NMR (300.1 MHz, $CD_3CN$): $\delta$ = 8.43 (m, 2 H), 8.17 (m, 2 H), 8.07-7.70 (m, 5 H), 7.61 (m, 1 H), 7.32 (m, 2 H), 7.19 (m, 1 H), 6.99 (m, 2 H), 6.53 (d with satellites, $J$(H,H) = 4.7 Hz, $J$(H,Pt) = 17.8 Hz, 1 H), 6.02 (dd with satellites, $J$(H,H) = 6.9, 2.3 Hz, $J$(H,Pt) = 20.2 Hz, 1 H), 5.78 (ddd with satellites, $J$(H,H) = 8.1, 2.3, 0.9 Hz, $J$(H,Pt) = 39 Hz, 1 H); $^{13}$C{$^1$H} NMR (75.45 MHz, $CD_3CN$): $\delta$ = 167.8-160.2 (several multiplets; C), 151.4 ($J$(C,Pt) = 16 Hz; CH), 150.1 (CH), 148.5 (CH), 144.6 (m; C), 144.2 (CH), 143.6 (CH), 143.4 (CH), 140.3 (m; C), 133.8 ($J$(C,Pt) = 32 Hz; CH), 132.2 ($J$(C,Pt) = 46 Hz; CH), 127.6-126.2 (m; CH), 125.1 ($J$(C,Pt) = 12 Hz; CH), 122.4 ($J$(C,Pt) = 12 Hz; CH), 114.3 (m; CH), 112.1 (m; CH), 104.5-103.0 (m; CH); elemental analysis calcd (%) for $C_{32}H_{19}F_7N_3O_{3.5}PtS_2$: C 43.01, H 2.14, N 4.70, S 7.18; found: C 42.94, H 2.08, N 5.05, S 7.38.

***mer*-3ad·H$_2$O.** Beige solid. Yield: 30%. $^1$H NMR (400.9 MHz, $CD_3CN$): $\delta$ = 9.04 (d, $J$(H,H) = 8.6 Hz, 1 H), 8.48-8.38 (m, 3 H), 8.21 (dd with satellites, $J$(H,H) = 6.1, 1.4 Hz, $J$(H,Pt) = 35.8 Hz, 1 H), 8.16-8.06 (m, 3 H), 7.99-7.89 (m, 2 H), 7.85 (d with satellites, $J$(H,H) = 6.3 Hz, $J$(H,Pt) = 11.2 Hz, 1 H), 7.80 (ddd with satellites, $J$(H,H) = 6.1, 1.4, 0.5 Hz, $J$(H,Pt) = 31.2 Hz, 1 H), 7.73 (d, $J$(H,H) = 6.3 Hz, 1 H), 7.45 (m, 1 H), 7.27 (m, 1 H), 7.20 (m, 2 H), 7.00 (m, 2 H), 6.88 (dd with satellites, $J$(H,H) = 7.4, 1.2 Hz, $J$(H,Pt) = 22.2 Hz, 1 H), 6.08 (dd with satellites, $J$(H,H) = 6.7, 2.3 Hz, $J$(H,Pt) = 19 Hz, 1 H), 5.78 (ddd with satellites, $J$(H,H) = 8.0, 2.2, 0.7 Hz, $J$(H,Pt) = 37.6 Hz, 1 H);$^{13}$C{$^1$H} NMR (100.81 MHz, $CD_3CN$): $\delta$ = 168.3-161.1 (several multiplets; C), 151.6 ($J$(C,Pt) = 16 Hz; CH), 148.7 (CH), 146.2 (C), 144.2 (C), 144.0 (CH), 143.2 (CH), 140.7 (CH), 140.0 (C), 134.7 (CH), 134.2-133.6 (m; CH), 131.2 (CH), 129.3 (CH), 129.2 (CH), 128.3 (C), 127.7 (CH), 127.4-126.6 (m; CH), 125.4 ($J$(C,Pt) = 14 Hz; CH), 114.5 (m; CH), 111.8 (m; CH), 104.0 ($J$(C,Pt) = 52 Hz; CH), 103.2 ($J$(C,Pt) = 54 Hz; CH); elemental analysis calcd (%) for $C_{38}H_{24}F_7N_3O_4PtS$: C 48.21, H 2.56, N 4.44, S 3.39; found: C 48.19, H 2.49, N 4.36, S 3.40.

***mer*-3bc·0.5CH$_2$Cl$_2$.** Beige solid. Yield: 64%. $^1$H NMR (400.9 MHz, $CD_3CN$): $\delta$ = 8.22 (m, 2 H), 8.12 (m, 2 H), 8.04-7.70 (m, 7 H), 7.56 (m, 1 H), 7.37-7.20 (m, 5

H), 7.16-7.07 (m, 2 H), 6.44 (dd with satellites, *J*(H,H) = 7.5, 0.7 Hz, *J*(H,Pt) = 15.6 Hz, 1 H), 6.41 (d with satellites, *J*(H,H) = 4.6 Hz, *J*(H,Pt) = 8.4 Hz, 1 H), 6.23 (dd with satellites, *J*(H,H) = 7.9, 0.8 Hz, *J*(H,Pt) = 31.8 Hz, 1 H); $^{13}C\{^1H\}$ NMR (100.81 MHz, $CD_3CN$): $\delta$ = 168.3 (C), 168.2 (C), 164.9 (C), 161.6 (C), 159.4 (C), 151.1 (*J*(C,Pt) = 16 Hz; CH), 149.7 (CH), 148.2 (CH), 144.6 (C), 143.3 (CH), 143.1 (CH), 142.4 (CH), 141.7 (C), 139.3 (C), 133.8-133.2 (CH), 132.6 (*J*(C,Pt) = 46 Hz; CH), 131.2 (*J*(C,Pt) = 24 Hz; CH), 128.4 (*J*(C,Pt) = 32 Hz; CH), 127.8 (CH), 127.5 (*J*(C,Pt) = 18 Hz; CH), 127.2 (*J*(C,Pt) = 30 Hz; CH), 127.0-126.8 (CH), 126.7 (*J*(C,Pt) = 28 Hz; CH), 124.7 (*J*(C,Pt) = 12 Hz; CH), 123.5 (*J*(C,Pt) = 30 Hz; CH), 123.1 (*J*(C,Pt) = 32 Hz; CH), 122.1 (*J*(C,Pt) = 12 Hz; CH); elemental analysis calcd (%) for $C_{32.5}H_{23}ClF_3N_3O_3PtS_2$: C 45.64, H 2.71, N 4.91, S 7.50; found: C 45.61, H 2.61, N 5.01, S 7.81.

***mer*-3bd·0.5H$_2$O.** Yellow solid. Yield: 35%. $^1$H NMR (400.9 MHz, $CD_3CN$): $\delta$ = 9.04 (d, *J*(H,H) = 8.5 Hz, 1 H), 8.45 (d, *J*(H,H) = 7.9 Hz, 1 H), 8.26-7.75 (m, 12 H), 7.68 (d, *J*(H,H) = 6.0 Hz, 1 H), 7.43-7.11 (m, 8 H), 6.82 (dd with satellites, *J*(H,H) = 7.3, 1.1 Hz, *J*(H,Pt) = 22 Hz, 1 H), 6.50 (dd with satellites, *J*(H,H) = 7.3, 0.8 Hz, *J*(H,Pt) = 14.6 Hz, 1 H), 6.22 (dd with satellites, *J*(H,H) = 7.9, 0.8 Hz, *J*(H,Pt) = 30.6 Hz, 1 H); $^{13}C\{^1H\}$ NMR (100.81 MHz, $CD_3CN$): $\delta$ = 168.7 (*J*(C,Pt) = 20 Hz; C), 168.4 (*J*(C,Pt) = 28 Hz; C), 164.8 (C), 164.7 (C), 162.3 (C), 151.2 (*J*(C,Pt) = 16 Hz; CH), 148.2 (CH), 146.7 (C), 144.5 (C), 143.2 (CH), 143.0 (C), 142.2 (CH), 141.5 (C), 140.5 (*J*(C,Pt) = 8 Hz; CH), 139.8 (C), 134.4 (CH), 134.3 (*J*(C,Pt) = 28 Hz; CH), 134.0-133.4 (m; CH), 133.3 (*J*(C,Pt) = 15 Hz; CH), 131.5 (*J*(C,Pt) = 24 Hz; CH), 131.0 (CH), 129.3 (CH), 129.1 (CH), 128.2 (C), 128.1 (*J*(C,Pt) = 30 Hz; CH), 127.7-126.7 (m; CH), 126.4 (*J*(C,Pt) = 30 Hz; CH), 124.9 (*J*(C,Pt) = 14 Hz; CH), 123.5 (*J*(C,Pt) = 30 Hz; CH), 123.2 (*J*(C,Pt) = 34 Hz; CH); elemental analysis calcd (%) for $C_{38}H_{28}F_3N_3O_4PtS$: C 52.17, H 3.23, N 4.80, S 3.67, found: C 51.91, H 3.23, N 5.03, S 3.70.

**Synthesis of *fac*-[Pt(dfppy)$_2$(ppy)]OTf (*fac*-3ab)**

A degassed solution of ***mer*-3ab** (204 mg, 0.232 mmol) in MeCN (350 mL) was irradiated in a UV photoreactor for 2 h. The solvent was removed under reduced pressure and the remaining residue was chromatographed on silica gel using a $CHCl_3$/MeOH mixture (9:1) as the eluent. Complex ***fac*-3ab**·0.5H$_2$O was isolated as an off-white solid after evaporation of the solvents. Yield: 131 mg, 64%. $^1$H NMR (400.9 MHz, $CD_3CN$): $\delta$ = 8.49 (m, 2 H), 8.30 (d, *J*(H,H) = 8.1 Hz, 1 H), 8.18 (m, 3 H), 7.97 (m, 1 H), 7.78-7.65 (m, 3 H), 7.43-7.34 (m, 4 H), 7.15 (m, 1 H), 6.98 (m, 2 H), 6.64 (dd with satellites, *J*(H,H) = 7.8, 0.8 Hz, *J*(H,Pt) = 43.4 Hz, 1 H), 6.24 (ddd with satellites, *J*(H,H) = 8.2, 2.4, 0.7 Hz, *J*(H,Pt) = 54 Hz, 1 H), 6.08 (ddd with satellites, *J*(H,H) = 8.3, 2.4, 0.7 Hz, *J*(H,Pt) = 53.4 Hz, 1 H); $^{13}C\{^1H\}$ NMR (100.81 MHz, $CD_3CN$): $\delta$ = 166.4-159.4 (several multiplets; C), 148.6 (m; CH), 144.6 (m; C), 143.4 (CH), 143.3 (CH), 143.1 (CH), 142.4 (C), 141.6 (C), 134.0 (*J*(C,Pt) = 54 Hz; CH), 132.6 (*J*(C,Pt) = 48 Hz; CH), 128.0-126.4 (m; CH), 123.4 (*J*(C,Pt) = 16 Hz; CH), 116.0 (m; CH), 103.8 (m; CH); elemental analysis calcd (%) for $C_{34}H_{21}F_7N_3O_{3.5}PtS$: C 46.00, H 2.38, N 4.73, S 3.61; found: C 46.07, H 2.53, N 4.96, S 3.47.

**Computational details**

Computational calculations were carried out with the Gaussian 09 package,[29] using the B3LYP hybrid functional,[30] together with the 6-31G**[31] basis set for the main-group elements and the LANL2DZ[32] double-$\zeta$ quality basis set and effective core potential for the platinum atom. The singlet ground-state geometries were optimized in the gas phase and in $CH_2Cl_2$ solution without symmetry restrictions. The solvent effect was computed by using the integral equation formalism variant of the polarizable continuum solvation model (IEFPCM).[33] Vertical excitation energies at the ground-state optimized geometry were obtained from time-dependent DFT (TD-DFT) as implemented in Gaussian 09, in the presence of the solvent ($CH_2Cl_2$). The lowest triplet state geometries were optimized in $CH_2Cl_2$ using the spin-unrestricted formalism (UB3LYP). All geometry optimizations were followed by vibrational frequency calculations to verify that the obtained geometries are minima on the potential energy surface.

## Acknowledgements

This work was supported by Ministerio de Economía y Competitividad, Spain (projects CTQ2011-24016 and CTQ2011-23862-C02 and FPU grant to F.J.). We are grateful to Prof. Antonio Guirado for providing the potentiostat/galvanostat.

**Keywords:** platinum • luminescence • density functional calculations • electrochemistry • cyclometalating ligands

[1] A. Vlček, *Coord. Chem. Rev.* **2000**, *200-202*, 933-978.

[2] L. Shi, W. Xia, *Chem. Soc. Rev.* **2012**, *41*, 7687-7697.

[3] (a) E. Baggaley, D. K. Cao, D. Sykes, S. W. Botchway, J. A. Weinstein, M. D. Ward, *Chem. Eur. J.* **2014**, *20*, 8898-8903; (b) E. Baggaley, J. A. Weinstein, J. A. G. Williams, *Coord. Chem. Rev.* **2012**, *256*, 1762-1785; (c) Y. You, S. Cho, W. Nam, *Inorg. Chem.* **2013**; (d) K. K.-W. Lo, A. W.-T. Choi, W. H.-T. Law, *Dalton Trans.* **2012**, *41*, 6021-6047; (e) D.-L. Ma, V. P.-Y. Ma, D. S.-H. Chan, K.-H. Leung, H.-Z. He, C.-H. Leung, *Coord. Chem. Rev.* **2012**, *256*, 3087-3113; (f) K. K.-W. Lo, K. H.-K. Tsang, K.-S. Sze, C.-K. Chung, T. K.-M. Lee, K. Y. Zhang, W.-K. Hui, C.-K. Li, J. S.-Y. Lau, D. C.-M. Ng, N. Zhu, *Coord. Chem. Rev.* **2007**, *251*, 2292-2310; (g) B. Higgins, B. A. DeGraff, J. N. Demas, *Inorg. Chem.* **2005**, *44*, 6662-6669.

[4] (a) R. Lincoln, L. Kohler, S. M. Monro, H. Yin, M. Stephenson, R. Zong, A. Chouai, C. L. Dorsey, R. Hennigar, R. P. Thummel, S. A. McFarland, *J. Am. Chem. Soc.* **2013**, *135*, 17161-17175; (b) A. Ruggi, F. W. B. van Leeuwen, A. H. Velders, *Coord. Chem. Rev.* **2011**, *255*, 2542-2554; (c) P. I. Djurovich, D. Murphy, M. E. Thompson, B. Hernandez, R. Gao, P. L. Hunt, M. Selke, *Dalton Trans.* **2007**, 3763-3770.

[5] P. T. Chou, Y. Chi, *Chem. Eur. J.* **2007**, *13*, 380-395.

[6] (a) H. Yersin, A. F. Rausch, R. Czerwieniec, T. Hofbeck, T. Fischer, *Coord. Chem. Rev.* **2011**, *255*, 2622-2652; (b) P.-T. Chou, Y. Chi, M.-W. Chung, C.-C. Lin, *Coord. Chem. Rev.* **2011**, *255*, 2653-2665; (c) E. O. Danilov, I. E. Pomestchenko, S. Kinayyigit, P. L. Gentili, M. Hissler, R. Ziessel, F. N. Castellano, *J. Phys. Chem. A* **2005**, *109*, 2465-2471.

[7] (a) N. M. Shavaleev, F. Monti, R. D. Costa, R. Scopelliti, H. J. Bolink, E. Ortí, G. Accorsi, N. Armaroli, E. Baranoff, M. Grätzel, M. K. Nazeeruddin, *Inorg. Chem.* **2012**, *51*, 2263-2271; (b) N. M. Shavaleev, F. Monti, R. Scopelliti, N. Armaroli, M. Grätzel, M. K. Nazeeruddin, *Organometallics* **2012**, *31*, 6288-6296; (c) N. M. Shavaleev, F. Monti, R. Scopelliti, A. Baschieri, L. Sambri, N. Armaroli, M. Grätzel, M. K. Nazeeruddin, *Organometallics* **2013**, *32*, 460-467; (d) A. Habibagahi, Y. Mebarki, Y. Sultan, G. P. A. Yap, R. J. Crutchley, *ACS Appl. Mater. Interfaces* **2009**, *1*, 1785-1792; (e) P. T. Chou, Y. Chi, *Eur. J. Inorg. Chem.* **2006**, 3319-3332; (f) J. Li, P. I. Djurovich, B. D. Alleyne, M. Yousufuddin, N. N. Ho, J. C. Thomas, J. C. Peters, R. Bau, M. E. Thompson, *Inorg. Chem.* **2005**, *44*, 1713-1727.

[8] (a) W. Leslie, A. S. Batsanov, J. A. Howard, J. A. Williams, *Dalton Trans.* **2004**, 623-631; (b) D. N. Kozhevnikov, V. N. Kozhevnikov, M. Z. Shafikov, A. M. Prokhorov, D. W. Bruce, J. A. Gareth Williams, *Inorg. Chem.* **2011**, *50*, 3804-3815.

[9] E. A. Medlycott, G. S. Hanan, *Coord. Chem. Rev.* **2006**, *250*, 1763-1782.

[10] (a) S. Monro, J. Scott, A. Chouai, R. Lincoln, R. Zong, R. P. Thummel, S. A. McFarland, *Inorg. Chem.* **2010**, *49*, 2889-2900; (b) N. D. McClenaghan, Y. Leydet, B. Maubert, M. T. Indelli, S. Campagna, *Coord. Chem. Rev.* **2005**, *249*, 1336-1350.

[11] (a) W. P. To, K. T. Chan, G. S. Tong, C. Ma, W. M. Kwok, X. Guan, K. H. Low, C. M. Che, *Angew. Chem. Int. Ed.* **2013**, *52*, 6648-6652; *Angew. Chem.* **2013**, *125*, 6780-6784; (b) W. P. To, G. S. Tong, W. Lu, C. Ma, J. Liu, A. L. Chow, C. M. Che, *Angew. Chem. Int. Ed.* **2012**, *51*, 2654-2657; *Angew. Chem.* **2013**, *124*, 2708-2711; (c) C. Bronner, O. S. Wenger, *Dalton Trans.* **2011**, *40*, 12409-12420.

[12] (a) P. K. Chow, C. Ma, W.-P. To, G. S. M. Tong, S.-L. Lai, S. C. F. Kui, W.-M. Kwok, C.-M. Che, *Angew. Chem. Int. Ed.* **2013**, *52*, 11775-11779; *Angew. Chem.* **2013**, *125*, 11991-11995; (b) P. K. Chow, W. P. To, K. H. Low, C. M. Che, *Chem. Asian J.* **2013**, *9*, 534-545.

[13] (a) L. Chassot, A. von Zelewsky, D. Sandrini, M. Maestri, V. Balzani, *J. Am. Chem. Soc.* **1986**, *108*, 6084-6085; (b) F. Barigelletti, D. Sandrini, M. Maestri, V. Balzani, A. von Zelewsky, L. Chassot, P. Jolliet, U. Maeder, *Inorg. Chem.* **1988**, *27*, 3644-3647; (c) D. M. Jenkins, S. Bernhard, *Inorg. Chem.* **2010**, *49*, 11297-11308; (d) M. La Deda, A. Crispini, I. Aiello, M. Ghedini, M. Amati, S. Belviso, F. Lelj, *Dalton Trans.* **2011**, *40*, 5259-5270; (e) E. Anger, M. Rudolph, L. Norel, S. Zrig, C. Shen, N. Vanthuyne, L.

Toupet, J. A. G. Williams, C. Roussel, J. Autschbach, J. Crassous, R. Reau, *Chem. Eur. J.* **2011**, *17*, 14178-14198.

[14] F. Juliá, D. Bautista, J. M. Fernández-Hernández, P. González-Herrero, *Chem. Sci.* **2014**, *5*, 1875-1880.

[15] S. Lamansky, P. Djurovich, D. Murphy, F. Abdel-Razzaq, R. Kwong, I. Tsyba, M. Bortz, B. Mui, R. Bau, M. E. Thompson, *Inorg. Chem.* **2001**, *40*, 1704-1711.

[16] (a) A. M. Bünzli, H. J. Bolink, E. C. Constable, C. E. Housecroft, J. M. Junquera-Hernández, M. Neuburger, E. Ortí, A. Pertegás, J. J. Serrano-Pérez, D. Tordera, J. A. Zampese, *Dalton Trans.* **2014**, *43*, 738-750; (b) A. Tsuboyama, H. Iwawaki, M. Furugori, T. Mukaide, J. Kamatani, S. Igawa, T. Moriyama, S. Miura, T. Takiguchi, S. Okada, M. Hoshino, K. Ueno, *J. Am. Chem. Soc.* **2003**, *125*, 12971-12979; (c) M. G. Colombo, T. C. Brunold, T. Riedener, H. U. Gudel, M. Fortsch, H. B. Burgi, *Inorg. Chem.* **1994**, *33*, 545-550.

[17] (a) D. N. Kozhevnikov, V. N. Kozhevnikov, M. M. Ustinova, A. Santoro, D. W. Bruce, B. Koenig, R. Czerwieniec, T. Fischer, M. Zabel, H. Yersin, *Inorg. Chem.* **2009**, *48*, 4179-4189; (b) J.-Y. Cho, B. Domercq, S. Barlow, K. Y. Suponitsky, J. Li, T. V. Timofeeva, S. C. Jones, L. E. Hayden, A. Kimyonok, C. R. South, M. Weck, B. Kippelen, S. R. Marder, *Organometallics* **2007**, *26*, 4816-4829.

[18] J. A. Garg, O. Blacque, T. Fox, K. Venkatesan, *Inorg. Chem.* **2010**, *49*, 11463-11472.

[19] (a) J. H. Seo, Y. K. Kim, Y. Ha, *Thin Solid Films* **2009**, *517*, 1807-1810; (b) G. Y. Park, J.-H. Seo, Y. K. Kim, Y. S. Kim, Y. Ha, *J. Korean Phys. Soc.* **2007**, *50*, 1729-1734.

[20] (a) Z. He, W.-Y. Wong, X. Yu, H.-S. Kwok, Z. Lin, *Inorg. Chem.* **2006**, *45*, 10922-10937; (b) Y. L. Chen, S. W. Li, Y. Chi, Y. M. Cheng, S. C. Pu, Y. S. Yeh, P. T. Chou, *ChemPhysChem* **2005**, *6*, 2012-2017.

[21] (a) J. V. Caspar, E. M. Kober, B. P. Sullivan, T. J. Meyer, *J. Am. Chem. Soc.* **1982**, *104*, 630-632; (b) E. M. Kober, J. V. Caspar, R. S. Lumpkin, T. J. Meyer, *J. Phys. Chem.* **1986**, *90*, 3722-3734; (c) J. S. Wilson, N. Chawdhury, M. R. A. Al-Mandhary, M. Younus, M. S. Khan, P. R. Raithby, A. Kohler, R. H. Friend, *J. Am. Chem. Soc.* **2001**, *123*, 9412-9417.

[22] C. M. Cardona, W. Li, A. E. Kaifer, D. Stockdale, G. C. Bazan, *Adv. Mater.* **2011**, *23*, 2367-2371.

[23] L. Chassot, A. von Zelewsky, *Inorg. Chem.* **1987**, *26*, 2814-2818.

[24] (a) S. I. Gorelsky, A. B. P. Lever, *Can. J. Anal. Sci. Spectr.* **2003**, *48*, 93-105; (b) A. B. P. Lever, S. I. Gorelsky, *Struct. Bonding (Berlin)* **2004**, *107*, 77-114; (c) Y. C. Chiu, C. H. Lin, J. Y. Hung, Y. Chi, Y. M. Cheng, K. W. Wang, M. W. Chung, G. H. Lee, P. T. Chou, *Inorg. Chem.* **2009**, *48*, 8164-8172; (d) K. Chen, C. H. Yang, Y. Chi, C. S. Liu, C. H. Chang, C. C. Chen, C. C. Wu, M. W. Chung, Y. M. Cheng, G. H. Lee, P. T. Chou, *Chem. Eur. J.* **2010**, *16*, 4315-4327; (e) B. S. Du, C. H. Lin, Y. Chi, J. Y. Hung, M. W. Chung, T. Y. Lin, G. H. Lee, K. T. Wong, P. T. Chou, W. Y. Hung, H. C. Chiu, *Inorg. Chem.* **2010**, *49*, 8713-8723.

[25] D. C. Powers, D. Benítez, E. Tkatchouk, W. A. Goddard, T. Ritter, *J. Am. Chem. Soc.* **2010**, *132*, 14092-14103.

[26] (a) J.-Y. Cho, K. Y. Suponitsky, J. Li, T. V. Timofeeva, S. Barlow, S. R. Marder, *J. Organomet. Chem.* **2005**, *690*, 4090-4093; (b) B. Ma, P. I. Djurovich, M. Yousufuddin, R. Bau, M. E. Thompson, *J. Phys. Chem. C* **2008**, *112*, 8022-8031; (c) H. Fukuda, Y. Yamada, D. Hashizume, T. Takayama, M. Watabe, *Appl. Organomet. Chem.* **2009**, *23*, 154-160.

[27] G. M. Sheldrick, *Acta Crystallogr., Sect. A: Found. Crystallogr.* **2008**, *64*, 112-122.

[28] (a) A. L. Spek, *J. Appl. Cryst.* **2003**, *36*, 7-13; (b) P. van der Sluis, A. L. Spek, *Acta Crystallogr., Sect. A: Found. Crystallogr.* **1990**, *46*, 194-201.

[29] M. J. Frisch, G. W. Trucks, H. B. Schlegel, G. E. Scuseria, M. A. Robb, J. R. Cheeseman, G. Scalmani, V. Barone, B. Mennucci, G. A. Petersson, H. Nakatsuji, M. Caricato, X. Li, H. P. Hratchian, A. F. Izmaylov, J. Bloino, G. Zheng, J. L. Sonnenberg, M. Hada, M. Ehara, K. Toyota, R. Fukuda, J. Hasegawa, M. Ishida, T. Nakajima, Y. Honda, O. Kitao, H. Nakai, T. Vreven, J. A. Montgomery, Jr., J. E. Peralta, F. Ogliaro, M. Bearpark, J. J. Heyd, E. Brothers, K. N. Kudin, V. N. Staroverov, R. Kobayashi, J. Normand, K. Raghavachari, A. Rendell, J. C. Burant, S. S. Iyengar, J. Tomasi, M. Cossi, N. Rega, N. J. Millam, M. Klene, J. E. Knox, J. B. Cross, V. Bakken, C. Adamo, J. Jaramillo, R. Gomperts, R. E. Stratmann, O. Yazyev, A. J. Austin, R. Cammi, C. Pomelli, J. W. Ochterski, R. L. Martin, K. Morokuma, V. G. Zakrzewski, G. A. Voth, P. Salvador, J. J. Dannenberg, S. Dapprich, A. D. Daniels, Ö. Farkas, J. B. Foresman, J. V. Ortiz, J. Cioslowski, D. J. Fox, Gaussian Inc., Wallingford CT, **2009**.

[30] (a) A. D. Becke, *Journal of Chemical Physics* **1993**, *98*, 5648-5652; (b) C. T. Lee, W. T. Yang, R. G. Parr, *Phys. Rev. B* **1988**, *37*, 785-789.

[31] (a) P. C. Hariharan, J. A. Pople, *Theoret. Chim. Acta* **1973**, *28*, 213-222; (b) M. M. Francl, W. J. Pietro, W. J. Hehre, J. S. Binkley, M. S. Gordon, D. J. Defrees, J. A. Pople, *J. Chem. Phys.* **1982**, *77*, 3654-3665.

[32] P. J. Hay, W. R. Wadt, *J. Chem. Phys.* **1985**, *82*, 299-310.

[33] J. Tomasi, B. Mennucci, R. Cammi, *Chem. Rev.* **2005**, *105*, 2999-3093.

Received: ((will be filled in by the editorial staff))
Revised: ((will be filled in by the editorial staff))
Published online: ((will be filled in by the editorial staff))

DOI: 10.1002/chem.201xxxxxx


**Entry for the Table of Contents**

Layout 2:

**FULL PAPER**

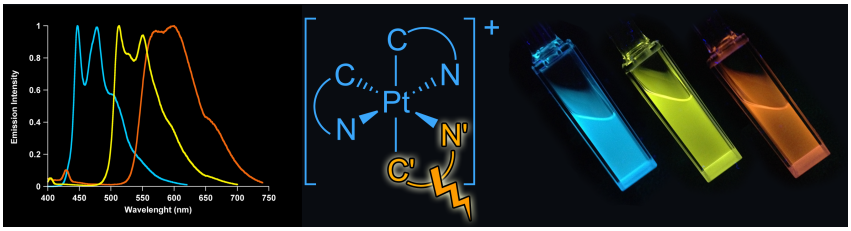


The long-lived $^3$LC emissions of tris-cyclometalated Pt$^{IV}$ complexes can be tuned from blue to orange through the variation of one the cyclometalating ligands. A combined experimental and DFT/TD-DFT study provides insight into the factors that determine the excited-state properties of this class of compounds.

**Luminescent Pt$^{IV}$ complexes**

*Fabio Juliá, Gabriel Aullón, Delia Bautista and Pablo González-Herrero**

■■ – ■■

**Exploring Excited-State Tunability in Luminescent Tris-cyclometalated Platinum(IV) Complexes: Synthesis of Heteroleptic Derivatives and Computational Calculations**